Electronic Supplementary Material (ESI) for Journal of Materials Chemistry A.

SUPPORTING INFORMATION

Transition metal nitrides doped catalysts (PdSn-TaN/C) as promising catalysts for high-performance methanol electrooxidation in alkaline medium

Table of Content

I. Additional information for DFT models

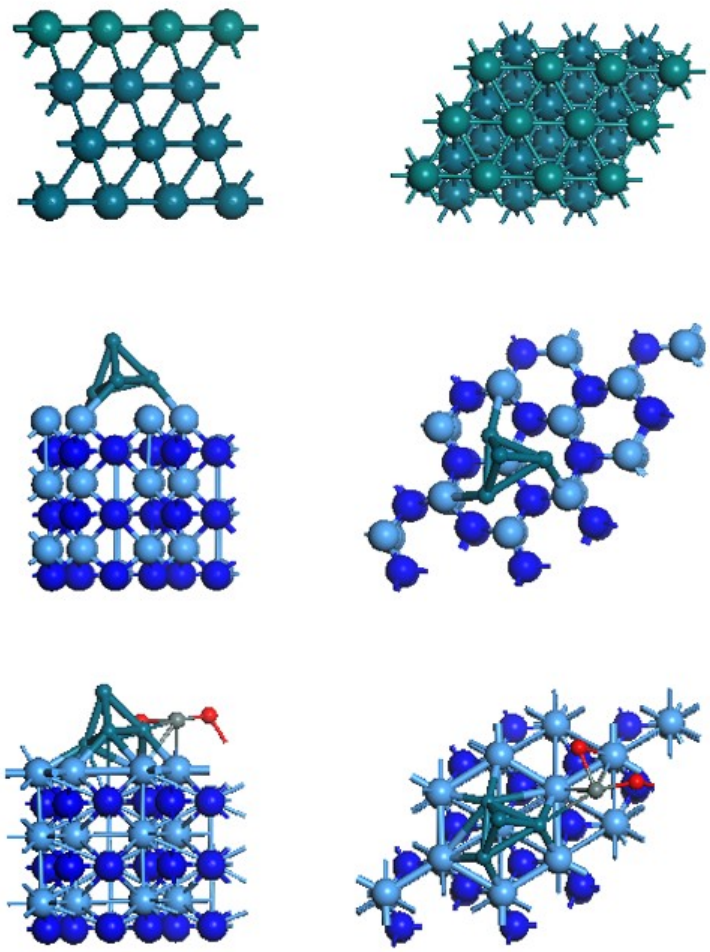

Figure S1. The stable configurations of Pd(111), Pd_4/TaN(001) and Pd_4-SnO_2/TaN(001) models.

II. Additional information for ICP-MS results

Table S1. The actual loading amounts and feed amounts of Pd_xSn_y-TaN/C and Pd_1Sn_3/C-m-alkaline catalysts.

Materials	Actual loading amount		Feed amount	
	Pd(wt%)	Sn(wt%)	Pd(wt%)	Sn(wt%)
Pd_1Sn_1-TaN/C-m-alkaline	2.95	2.92	3.33	3.71
Pd_1Sn_3-TaN/C-w-alkaline	3.15	9.89	3.33	11.13
Pd_1Sn_3-TaN/C-m-alkaline	3.44	10.13	3.33	11.13
Pd_1Sn_3-TaN/C-s-alkaline	3.24	9.18	3.33	11.13
Pd-TaN/C-m-alkaline	3.43	0	3.33	0
Pd_1Sn_3/C-m-alkaline	3.13	8.99	3.33	11.13

III. Additional information for TEM fitting

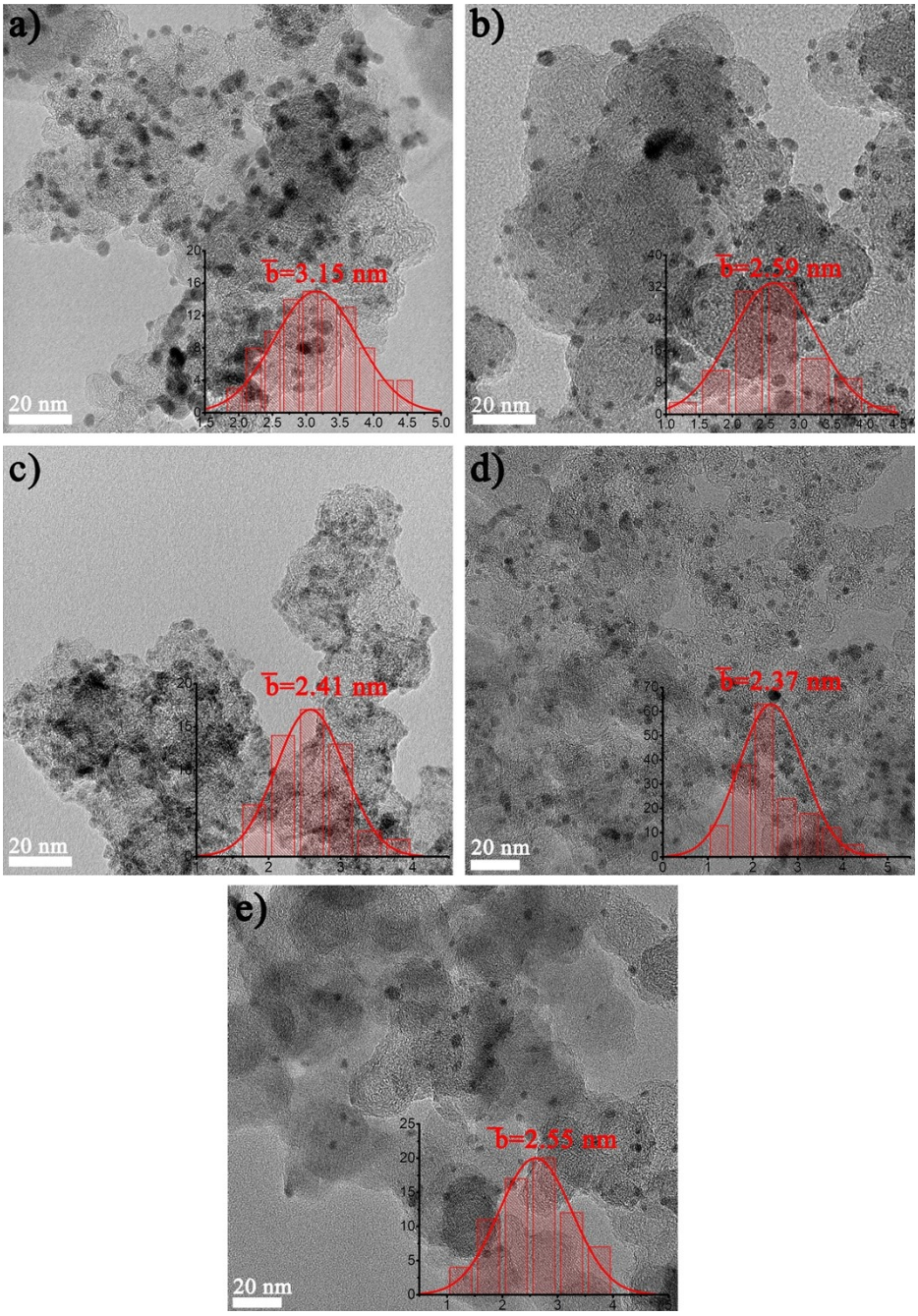

Figure S2. TEM images of the Pd_1Sn_1-TaN/C-m-alkaline (a), Pd_1Sn_3-TaN/C-w-alkaline (b), Pd_1Sn_3-TaN/C-s-alkaline (c), Pd-TaN/C-m-alkaline (d) and Pd_1Sn_3--m-alkaline (e).

IV. Additional information for XPS fitting

Table S2. XPS elemental analysis of Pd in the Pd_xSn_y-TaN/C catalysts.

Materials	Atomic percentage			
	Pd		$Pd^{\delta+}$	
Pd_1Sn_1-TaN/C-m-alkaline	83.98 %	335.36 eV	16.01 %	337.24 eV
Pd_1Sn_3-TaN/C-w-alkaline	78.51 %	335.42 eV	21.49 %	337.38 eV
Pd_1Sn_3-TaN/C-m-alkaline	74.81 %	335.19 eV	25.19 %	337.11 eV
Pd_1Sn_3-TaN/C-s-alkaline	55.14 %	335.64 eV	44.87 %	337.64 eV
Pd-TaN/C-m-alkaline	86.48 %	335.98 eV	13.51 %	337.78 eV
Pd_1Sn_3/C-m-alkaline	70.54 %	335.29 eV	29.46 %	337.30 eV

Table S3. XPS elemental analysis of Sn in the Pd_xSn_y-TaN/C catalysts.

Materials	Atomic percentage			
	Sn		$Sn^{\delta+}$	
Pd_1Sn_3-TaN/C-w-alkaline	16.75%	484.52 eV	83.25%	486.73 eV
Pd_1Sn_1-TaN/C-m-alkaline	27.33%	485.11 eV	72.67%	486.9 eV
Pd_1Sn_3-TaN/C-m-alkaline	12.37%	484.38 eV	87.63%	486.2 eV
Pd_1Sn_3-TaN/C-s-alkaline	6.87%	485.11 eV	93.13%	486.75 eV

Table S4. XPS elemental analysis of Ta in the Pd_xSn_y-TaN/C catalysts.

Materials	Atomic percentage			
	O-Ta-O	O-Ta-N		N-Ta-N
Pd_1Sn_3-TaN/C-w-alkaline	29.17%	50.59%	26.66 eV	20.24%
Pd_1Sn_1-TaN/C-m-alkaline	17.95%	63.58%	26.14 eV	18.47%
Pd_1Sn_3-TaN/C-m-alkaline	32.37%	54.61%	26.39 eV	13.03%
Pd_1Sn_3-TaN/C-s-alkaline	37.43%	51.91%	25.69 eV	10.67%
Pd-TaN/C-m-alkaline	32.78%	49.07%	25.70 eV	18.15%

V. Additional information for Electrochemical studies (MOR)

Table S5. Comparison of PdSn/TaN-C with previous reported Pd-based catalysts towards MOR in alkaline medium.

Materials	Electrolyte	Mass activity ($A\ g_{metal}^{-1}$)	CA test (s)	Residual current ($A\ g_{metal}^{-1}$)	ref
PdCuM (M = Ru, Rh, Ir)	1 M KOH + 1 M CH_3OH	1660.8	3000	< 100	[1]
Pd-PdO PNT	1 M KOH + 1 M CH_3OH	1111.3	3600	< 20	[2]
Pd/NL-GCN	0.5 M NaOH + 1 M CH_3OH	816.5	3000	150	[3]
Pd_3Cu_1	1 M KOH + 1 M CH_3OH	600	3600	< 25	[4]
$Pt_{84}Pd_{16}$	0.1 M KOH + 1 M CH_3OH	999	3000	< 200	[5]
PdCo nanowire	1 M KOH + 1 M CH_3OH	1205	2000	< 30	[6]
$Pd_{20-x}Ag_x$/CNT	1 M KOH + 0.5 M CH_3OH	731	2000	< 220	[7]
PdCu nanocages	0.5 M KOH + 1 M CH_3OH	823	6000 (3600)	50 (< 100)	[8]
PdSn	1 M KOH + 1 M CH_3OH	1109.1	4000	67.8	[9]
PdPt	1 M KOH + 0.5 M CH_3OH	1130	4000	151.7	[10]
PtRu nanowires	0.1 M KOH + 0.5 M CH_3OH	820	4000	~200	[11]
Pd/SiO_2@RGO	1 M KOH + 1 M CH_3OH	1533	1500	308.5	[12]
PtCuPd@PdCu@Ru	1 M KOH + 2 M CH_3OH	2480	6000	< 350	[13]
Pd-CeO_2	1 M KOH + 1 M CH_3OH	1500	3000	109.4	[14]
Commercial PtRu/C	1 M KOH + 1 M CH_3OH	260	3000	61.1	[14]
PdSn/TaN-C	1 M KOH + 1 M CH_3OH	3293.46	3600	501.0	**This work**

VI. Additional information for EIS fitting

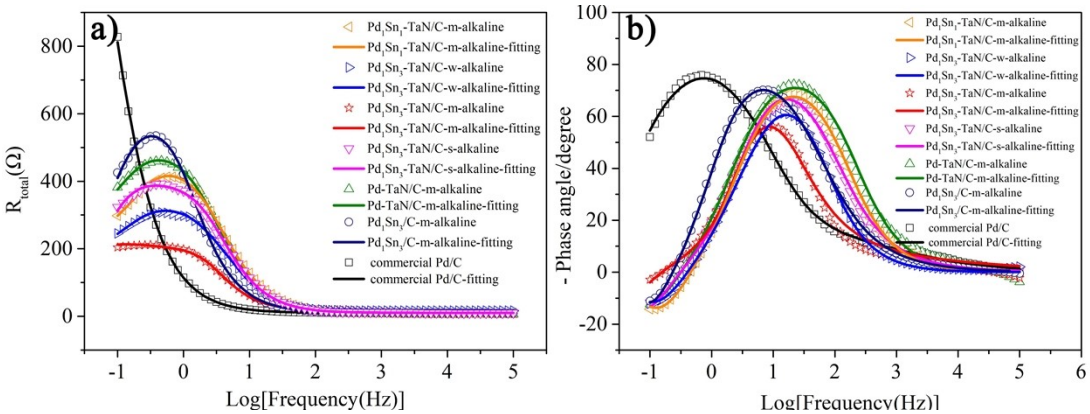

Figure S3. The corresponding bode plots for MOR in alkaline medium.

Table S6. Kinetic parameters of Pd_xSn_y-TaN/C, Pd_1Sn_3/C-m-alkaline and commercial Pd/C towards alkaline MOR.

Materials	R_s (Ω)	R_{ct} (Ω)
Pd_1Sn_1-TaN/C-m-alkaline	9.9	427.6
Pd_1Sn_3-TaN/C-w-alkaline	16.7	302.2
Pd_1Sn_3-TaN/C-m-alkaline	10.6	200.2
Pd_1Sn_3-TaN/C-s-alkaline	9.97	334.9
Pd-TaN/C-m-alkaline	6.4	477.2
Pd_1Sn_3/C-m-alkaline	9.6	645.2
Commercial Pd/C	6.5	1690.0

VII. Additional information for in-situ FTIR studies

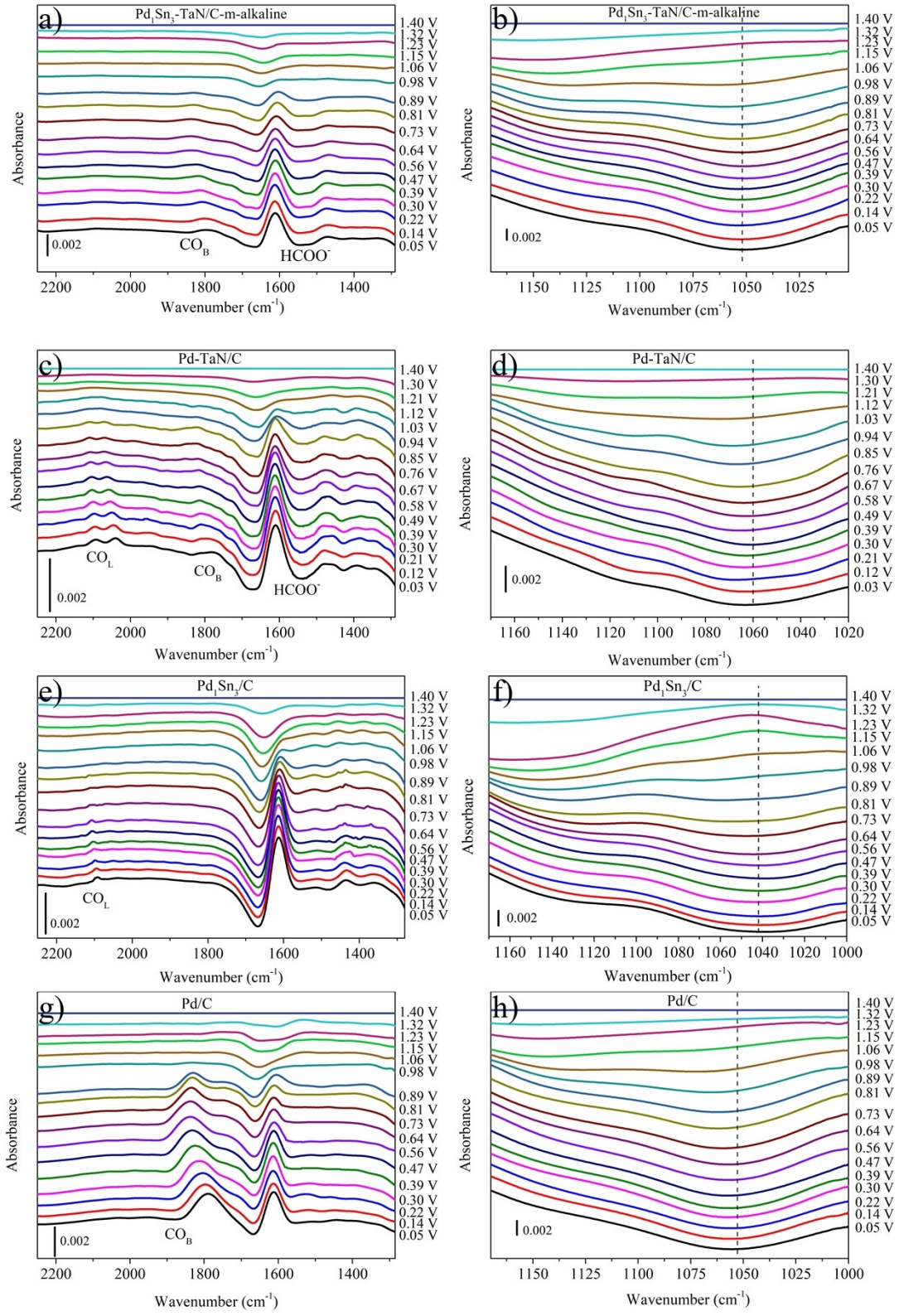

Figure S4. The in-situ FTIR characterization of PdSn/TaN-C **(a,b)**, Pd/TaN-C **(c,d)**, PdSn/C **(e, f)** and commercial Pd/C **(g, h)**. (the reference spectra are recorded at 1.4 V, where the CO_{ad} is suppressed; the dash lines in **Figure S4(b, d, f, h)** represent the band at around 1050 cm^{-1}.)

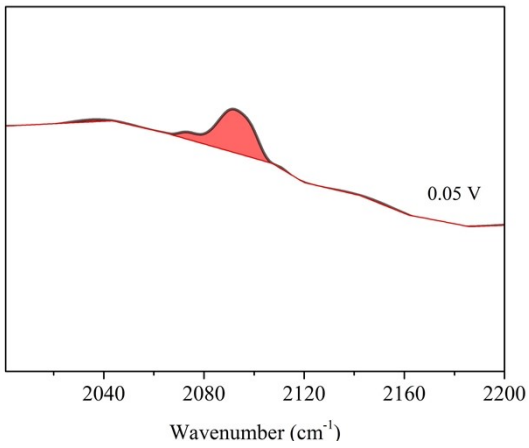

Figure S5. The CO area fit (intensity) of a peak at 0.05V (with the spectrum at 1.4 V as the reference) in **Figure S4(e)** for PdSn/C.

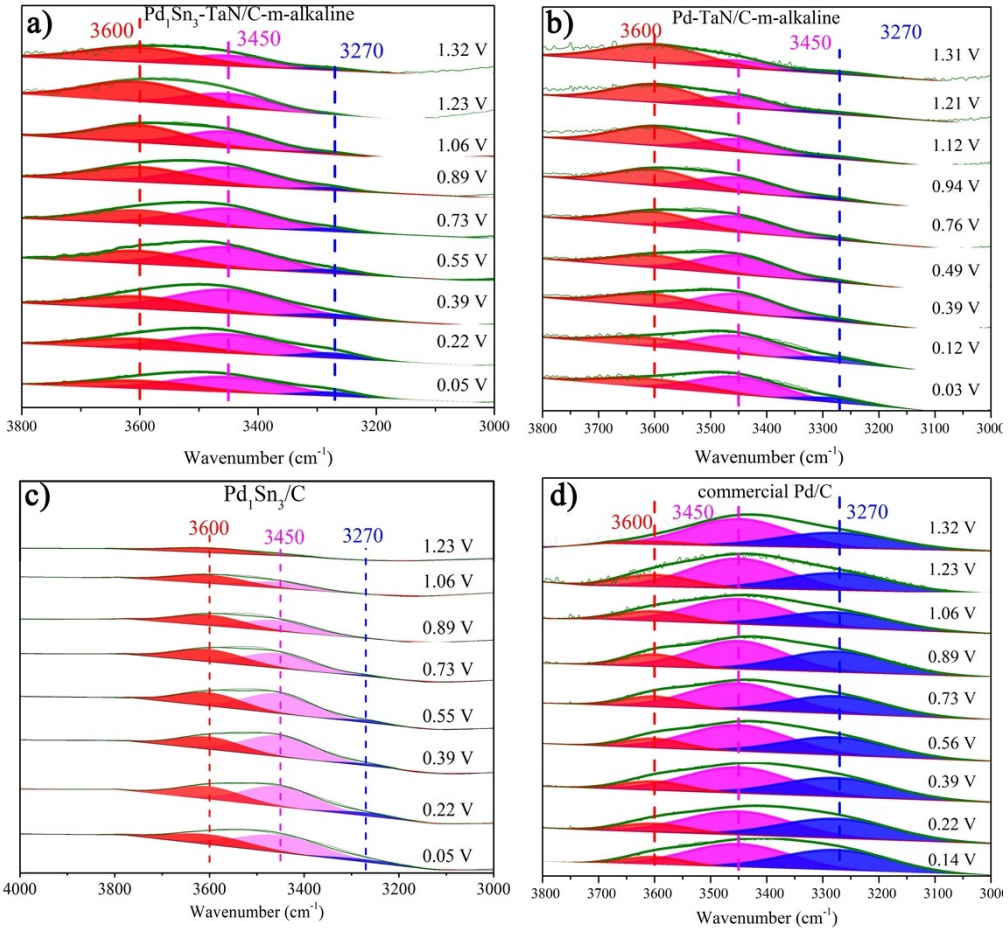

Figure S6. The fitting results of H_2O features band on Pd_1Sn_3-TaN/C-m-alkaline(a), Pd-TaN/C(b), Pd_1Sn_3/C(c) and commercial Pd/C(d) in the range of 3000 to 3800 cm^{-1}.

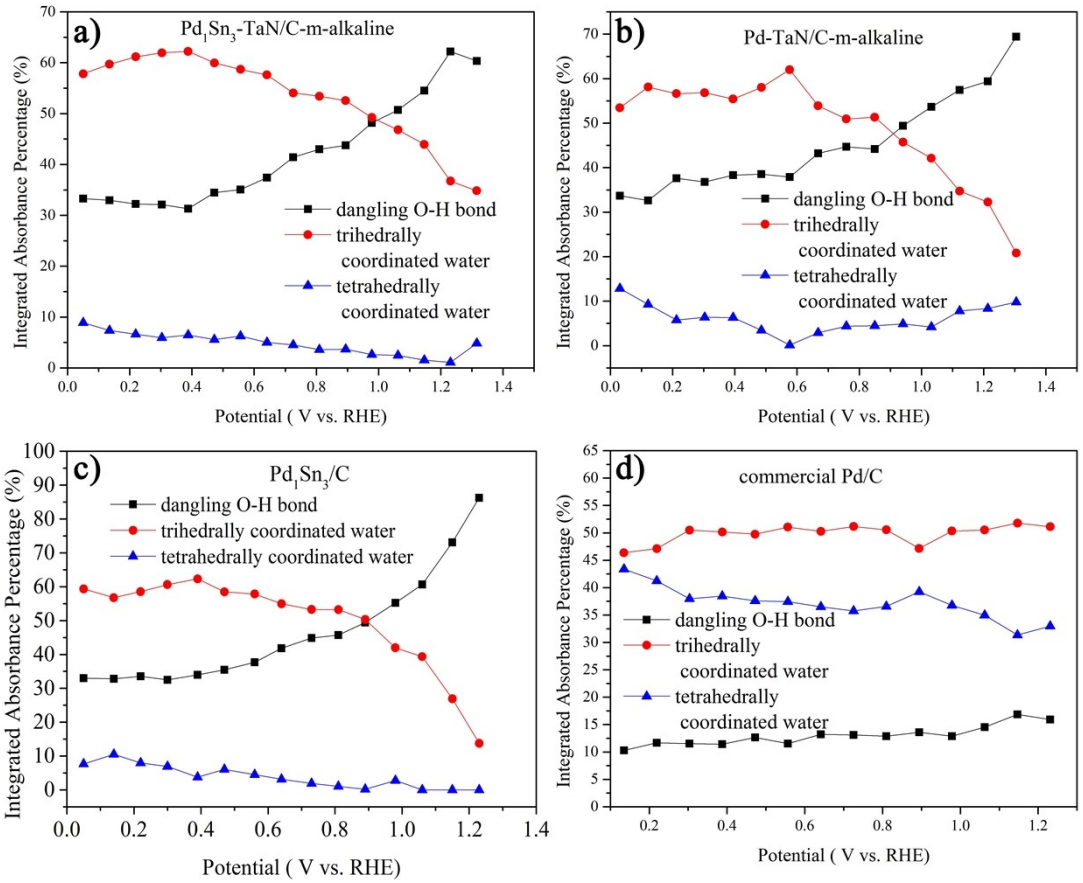

Figure S7. In-situ FTIR study on the integrated intensities percentage of H_2O band fitting results on Pd_1Sn_3-TaN/C-m-alkaline(a), Pd-TaN/C(b), Pd_1Sn_3/C(c) and commercial Pd/C(d) catalysts.

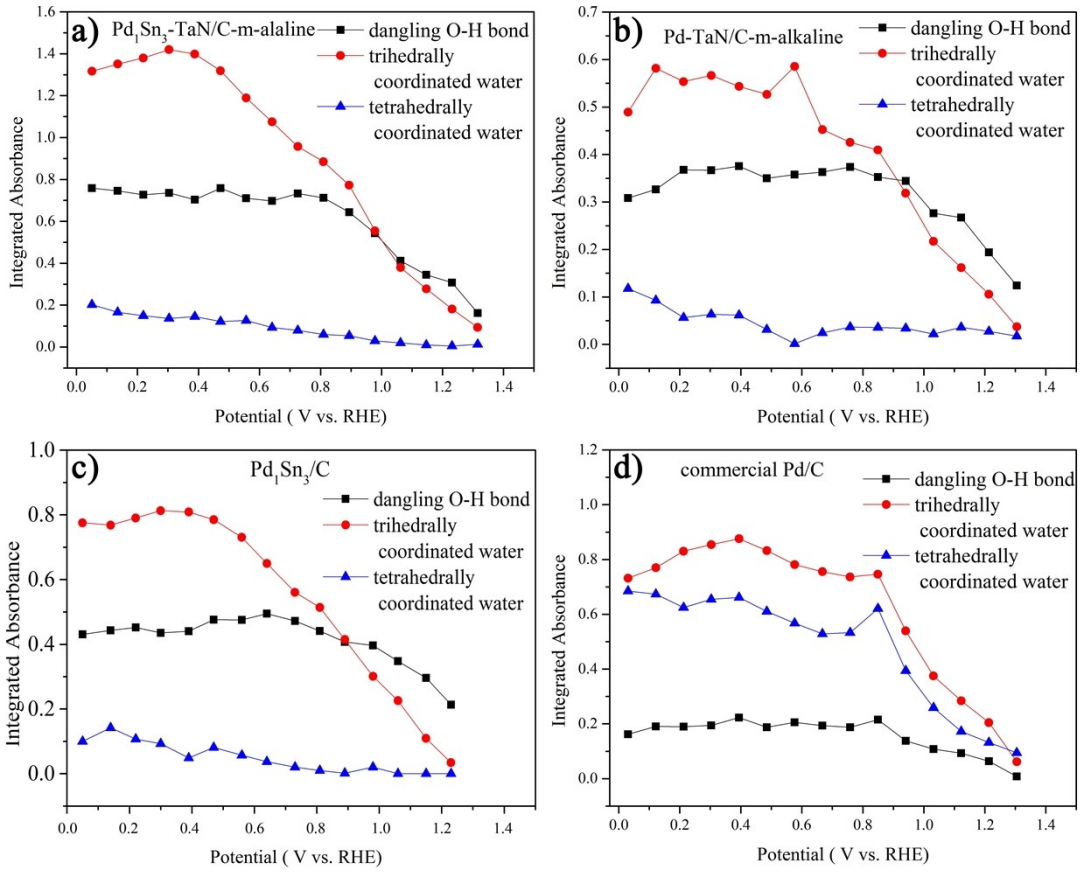

Figure S8. In-situ FTIR study on the potential dependence of the integrated intensities of H_2O band fitting results on Pd_1Sn_3-TaN/C-m-alkaline(a), Pd-TaN/C(b), Pd_1Sn_3/C(c) and commercial Pd/C(d) catalysts.

Table S7. In-situ FTIR fitting analysis of H_2O in the PdSn-TaN/C catalysts.

Potentials	dangling O-H bond		trihedrally coordinated water		tetrahedrally coordinated water	
(V)	Area Fit (intensity)	Area Fit(%)	Area Fit (intensity)	Area Fit (%)	Area Fit (intensity)	Area Fit (%)
0.05	0.758	33.294	1.317	57.817	0.202	8.889
0.14	0.745	32.945	1.351	59.712	0.166	7.344
0.22	0.727	32.214	1.380	61.167	0.149	6.619
0.30	0.736	32.115	1.420	61.941	0.136	5.944
0.39	0.703	31.294	1.399	62.229	0.146	6.477
0.47	0.758	34.471	1.319	59.974	0.122	5.555
0.56	0.710	35.061	1.189	58.699	0.126	6.240
0.64	0.698	37.395	1.075	57.593	0.094	5.012
0.73	0.733	41.420	0.957	54.063	0.080	4.517
0.81	0.712	42.993	0.885	53.410	0.060	3.597
0.89	0.643	43.770	0.772	52.550	0.054	3.680
0.98	0.543	48.164	0.555	49.226	0.029	2.611
1.06	0.411	50.735	0.379	46.798	0.020	2.467
1.15	0.345	54.510	0.278	43.944	0.010	1.545
1.23	0.308	62.211	0.182	36.720	0.005	1.069
1.32	0.162	60.333	0.093	34.833	0.013	4.835

Table 8. In-situ FTIR fitting analysis of H_2O in the Pd-TaN/C catalysts.

Potentials	dangling O-H bond		trihedrally coordinated water		tetrahedrally coordinated water	
(V)	Area Fit (intensity)	Area Fit(%)	Area Fit (intensity)	Area Fit (%)	Area Fit (intensity)	Area Fit (%)
0.03	0.308	33.704	0.489	53.448	0.118	12.847
0.12	0.326	32.610	0.582	58.110	0.093	9.280
0.21	0.368	37.599	0.553	56.620	0.057	5.781
0.30	0.367	36.792	0.566	56.832	0.064	6.376
0.39	0.376	38.292	0.543	55.411	0.062	6.297
0.49	0.350	38.541	0.527	58.015	0.031	3.444
0.58	0.358	37.868	0.585	61.999	0.001	0.132
0.67	0.363	43.204	0.452	53.886	0.024	2.910
0.76	0.374	44.697	0.426	50.940	0.036	4.363
0.85	0.353	44.198	0.409	51.320	0.036	4.482
0.94	0.345	49.413	0.319	45.705	0.034	4.882
1.03	0.276	53.662	0.217	42.135	0.022	4.202
1.12	0.267	57.447	0.162	34.743	0.036	7.810
1.21	0.194	59.364	0.106	32.268	0.027	8.368
1.30	0.124	69.410	0.037	20.807	0.017	9.784

Table S9. In-situ FTIR fitting analysis of H_2O in the PdSn/C catalysts.

Potentials	dangling O-H bond		trihedrally coordinated water		tetrahedrally coordinated water	
(V)	Area Fit (intensity)	Area Fit(%)	Area Fit (intensity)	Area Fit (%)	Area Fit (intensity)	Area Fit (%)
0.05	0.431	32.983	0.775	59.361	0.100	7.655
0.14	0.443	32.756	0.768	56.778	0.142	10.466
0.22	0.452	33.505	0.790	58.555	0.107	7.940
0.30	0.436	32.467	0.813	60.615	0.093	6.918
0.39	0.441	33.945	0.809	62.319	0.048	3.735
0.47	0.476	35.461	0.785	58.484	0.081	6.055
0.56	0.475	37.637	0.730	57.845	0.057	4.518
0.64	0.495	41.861	0.650	54.989	0.037	3.151
0.73	0.472	44.838	0.561	53.262	0.020	1.900
0.81	0.441	45.716	0.514	53.259	0.010	1.024
0.89	0.407	49.458	0.415	50.356	0.002	0.186
0.98	0.396	55.248	0.301	41.964	0.020	2.789
1.06	0.347	60.650	0.225	39.350	0.000	0.000
1.15	0.296	73.094	0.109	26.906	0.000	0.000
1.23	0.213	86.262	0.034	13.738	0.000	0.000

Table S10. In-situ FTIR fitting analysis of H_2O in the Pd/C catalysts.

Potentials	dangling O-H bond		trihedrally coordinated water		tetrahedrally coordinated water	
(V)	Area Fit (intensity)	Area Fit(%)	Area Fit (intensity)	Area Fit (%)	Area Fit (intensity)	Area Fit (%)
0.05	0.150	9.490	0.720	45.570	0.710	44.940
0.14	0.162	10.279	0.732	46.363	0.685	43.358
0.22	0.190	11.656	0.770	47.115	0.674	41.229
0.30	0.190	11.527	0.831	50.505	0.624	37.969
0.39	0.194	11.402	0.854	50.163	0.655	38.435
0.47	0.223	12.666	0.876	49.756	0.661	37.578
0.56	0.188	11.517	0.832	51.051	0.610	37.432
0.64	0.205	13.217	0.782	50.282	0.567	36.501
0.73	0.193	13.084	0.756	51.150	0.528	35.766
0.81	0.187	12.864	0.736	50.553	0.533	36.583
0.89	0.215	13.586	0.746	47.158	0.621	39.256
0.98	0.138	12.881	0.539	50.341	0.394	36.778
1.06	0.108	14.529	0.375	50.526	0.259	34.945
1.15	0.093	16.867	0.284	51.771	0.172	31.361
1.23	0.064	15.913	0.205	51.127	0.132	32.960
1.30	0.008	4.898	0.062	37.562	0.095	57.540

VIII. Additional information for DFT calculations

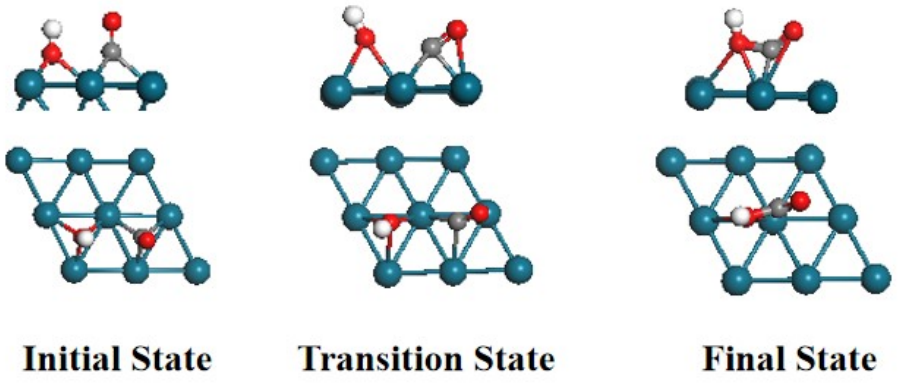

Figure S9. The configurations of the initial state, transition state and final state of the reaction CO+OH→COOH on the Pd(111) surface

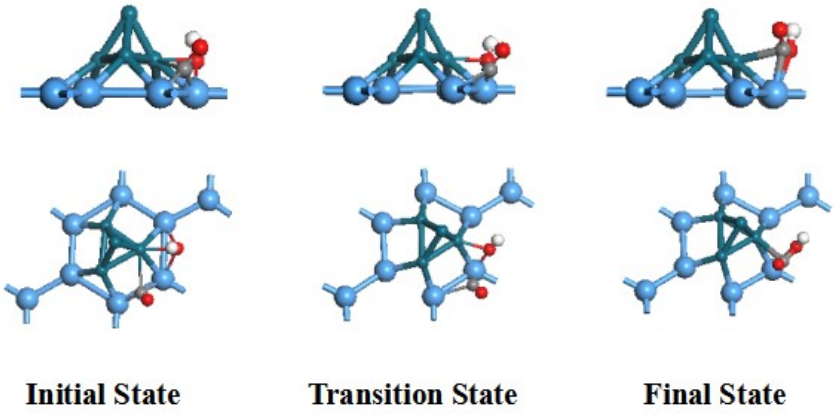

Figure S10. The configurations of the initial state, transition state and final state of the reaction CO+OH→COOH on the Pd_4/TaN(001) surface

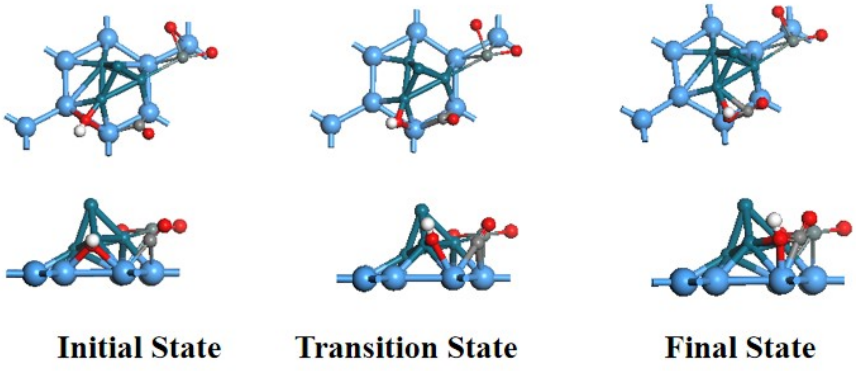

Figure S11. The configurations of the initial state, transition state and final state of the reaction CO+OH→COOH on the Pd_4-SnO_2/TaN(001) surface

IX. Additional information for Electrochemical studies towards TaN/C and FAOR

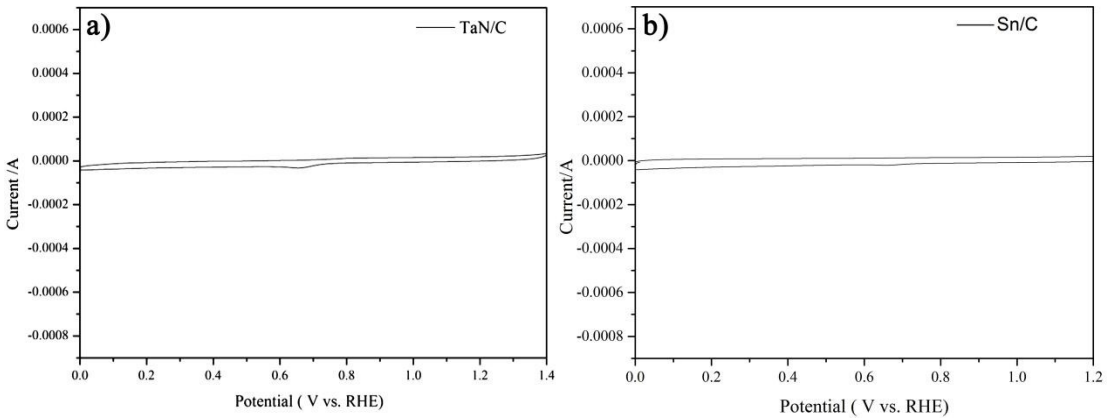

Figure S12. CV curves of pure TaN/C (a) and Sn/C (b)catalyst in Ar-saturated 1 M CH_3OH and 1M KOH with a sweep rate of 50 mv^{-1}.

Table S11. The catalytic performances of the Pd_xSn_y/TaN-C, Pd_1Sn_3/C-m-alkaline and commercial Pd/C for FAOR in acid medium

Materials	ECSA	FAOR	
	(m^2 g^{-1})	I_p(m)/(mA mg_{Pd}^{-1})	I_p(sa)/(mA cm_{Pd}^{-2})
Pd_1Sn_3-TaN/C-m-alkaline	203.99	2097.29	1.03
Pd-TaN/C-m-alkaline	119.45	1036.68	0.86
Pd_1Sn_3/C-m-alkaline	70.18	103.67	0.15
Commercial Pd/C	42.23	215.79	0.51

Table S12. Comparison of PdSn/TaN-C with previous reported Pd-based catalysts towards FAOR in acidic medium.

Materials	Electrolyte	Mass activity ($A\ g_{metal}^{-1}$)	CA test (s)	Residual current ($A\ g_{metal}^{-1}$)	ref
Pd/NL-GCN	0.5 M NaOH + 1 M CH_3OH	1310.0	1000	< 50	[3]
Pd-Mo_2N/rGO	0.5 M H_2SO_4 + 0.5 M HCOOH	532.7	3600	32.3	[15]
Pd/rGO	0.5 M H_2SO_4 + 0.5 M HCOOH	313.4	3600	6.6	[15]
Pd/VC	0.5 M H_2SO_4 + 0.5 M HCOOH	243.4	3600	2.7	[15]
PdNi nanowire/rGO	0.5 M H_2SO_4 + 0.5 M HCOOH	604.3	2000	13	[16]
PdNiCu/C	0.5 M H_2SO_4 + 0.5 M HCOOH	792	3600	< 10	[17]
PdNi hollow nanocrystals	0.5 M H_2SO_4 + 0.5 M HCOOH	768	3600	0.2	[18]
Pd_3Fe/C	0.5 M H_2SO_4 + 0.5 M HCOOH	696.4	3000	< 50	[19]
PtAgCu@PtCu	0.5 M H_2SO_4 + 0.5 M HCOOH	314	3000	< 40	[20]
Pd nanosheets	0.5 M H_2SO_4 + 0.5 M HCOOH	409.3	3000	28.2	[21]
Pd@Ni-B/C	0.5 M H_2SO_4 + 0.5 M HCOOH	400	4000	< 50	[22]
Pd_3Sn_2	0.5 M $HClO_4$ + 0.5 M HCOOH	448	6000 (3600)	< 5 (< 10)	[23]
Pd	0.5 M $HClO_4$ + 0.5 M HCOOH	630	2000	< 30	[24]
PdSn/TaN-C	0.5 M H_2SO_4 + 0.5 M HCOOH	2097.29	3600	60	**This work**

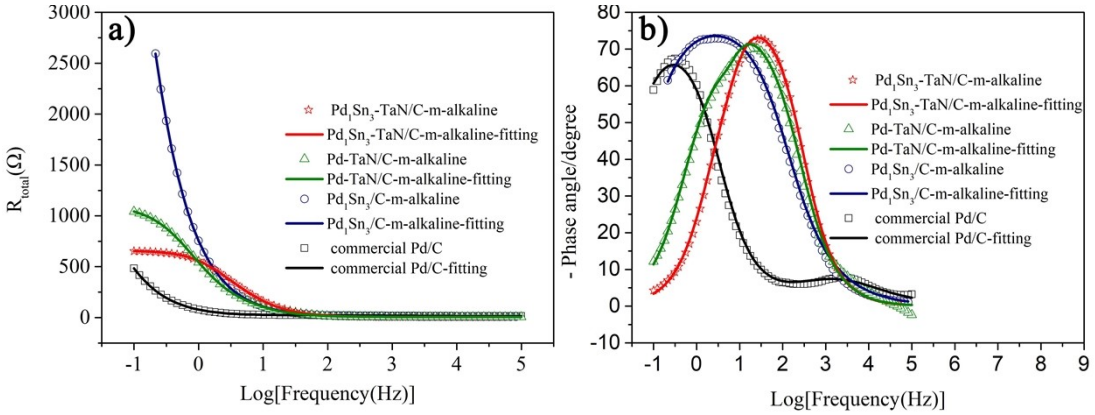

Figure S13. The corresponding bode plots for FAOR in acidic medium.

Table S13. Kinetic parameters of Pd_xSn_y-TaN/C, Pd_1Sn_3/C-m-alkaline and commercial Pd/C towards acidic FAOR.

Materials	R_s (Ω)	R_{ct} (Ω)
Pd_1Sn_3-TaN/C-m-alkaline	6.8	597.7
Pd-TaN/C-m-alkaline	5.8	1089
Pd_1Sn_3/C-m-alkaline	8.3	9066
Commercial Pd/C	14.11	1751

References:

[1] L. Jin, H. Xu, C. Chen, et al, Three-dimensional PdCuM (M = Ru, Rh, Ir) Trimetallic Alloy Nanosheets for Enhancing Methanol Oxidation Electrocatalysis, ACS Appl. Mater. Inter. 11 (2019) 42123-42130.

[2] T.J. Wang, F.M. Li, H. Huang, et al, Porous Pd-PdO Nanotubes for Methanol Electrooxidation, Adv. Funct. Mater. 30 (2020) 2000534.

[3] H. Huang, Y. Wei, B. Shen, et al, Synthesis of Multiple-Twinned Pd Nanoparticles Anchored on Graphitic Carbon Nanosheets for Use as Highly-Active Multifunctional Electrocatalyst in Formic Acid and Methanol Oxidation Reactions, Advanced Materials Interfaces. 7 (2020) 2000142.

[4] A. Serov, T. Asset, M. Padilla, et al, Highly-active Pd-Cu electrocatalysts for oxidation of ubiquitous oxygenated fuels, Applied Catalysis B: Environmental. 191 (2016) 76-85.

[5] V. Nguyen, Q.C. Tran, N.D. Quang, et al, N-doped Cdot/PtPd nanonetwork hybrid materials as highly efficient electrocatalysts for methanol oxidation and formic acid oxidation reactions, J. Alloy. Compd. 766 (2018) 979-986.

[6] C. Wang, L. Zheng, R. Chang, et al, Palladium-Cobalt Nanowires Decorated with Jagged Appearance for Efficient Methanol Electro-oxidation, ACS Appl. Mater. Inter. 10 (2018) 29965-

29971.

[7] M. Satyanarayana, G. Rajeshkhanna, M.K. Sahoo, et al, Electrocatalytic Activity of $Pd_{20-x}Ag_x$ Nanoparticles Embedded in Carbon Nanotubes for Methanol Oxidation in Alkaline Media, ACS Applied Energy Materials. 1 (2018) 3763-3770.

[8] Z. Chen, Y. He, J. Chen, et al, PdCu Alloy Flower-like Nanocages with High Electrocatalytic Performance for Methanol Oxidation, The Journal of Physical Chemistry C. 122 (2018) 8976-8983.

[9] H. Shang, H. Xu, C. Wang, et al, General synthesis of Pd-pm (pm = Ga, In, Sn, Pb, Bi) alloy nanosheet assemblies for advanced electrocatalysis, Nanoscale. 12 (2020) 3411-3417.

[10] T. Guo, H. Xiang, W. Li, et al, Synthesis of Ultrathin and Composition-Tunable PdPt Porous Nanowires with Enhanced Electrocatalytic Performance, ACS Sustain. Chem. Eng. 8 (2020) 2901-2909.

[11] L. Huang, X. Zhang, Q. Wang, et al, Shape-Control of Pt-Ru Nanocrystals: Tuning Surface Structure for Enhanced Electrocatalytic Methanol Oxidation, J. Am. Chem. Soc. 140 (2018) 1142-1147.

[12] F. Yang, B. Zhang, S. Dong, et al, Silica nanosphere supported palladium nanoparticles encapsulated with graphene: High-performance electrocatalysts for methanol oxidation reaction, Appl. Surf. Sci. 452 (2018) 11-18.

[13] F. Saleem, Z. Zhang, X. Cui, et al, Elemental Segregation in Multimetallic Core-Shell Nanoplates, J. Am. Chem. Soc. 141 (2019) 14496-14500.

[14] Q. Tan, C. Shu, J. Abbott, et al, Highly Dispersed Pd-CeO_2 Nanoparticles Supported on N-Doped Core-Shell Structured Mesoporous Carbon for Methanol Oxidation in Alkaline Media, ACS Catal. 9 (2019) 6362-6371.

[15] H. Yan, Y. Jiao, A. Wu, et al, Synergism of molybdenum nitride and palladium for high-efficiency formic acid electrooxidation, J. Mater. Chem. A. 6 (2018) 7623-7630.

[16] D. Bin, B. Yang, F. Ren, et al, Facile synthesis of PdNi nanowire networks supported on reduced graphene oxide with enhanced catalytic performance for formic acid oxidation, J. Mater. Chem. A. 3 (2015) 14001-14006.

[17] S. Hu, F. Munoz, J. Noborikawa, et al, Carbon supported Pd-based bimetallic and trimetallic catalyst for formic acid electrochemical oxidation, Applied Catalysis B: Environmental. 180 (2016) 758-765.

[18] Z. Chen, J. Zhang, Y. Zhang, et al, NiO-induced synthesis of PdNi bimetallic hollow nanocrystals with enhanced electrocatalytic activities toward ethanol and formic acid oxidation, Nano Energy. 42 (2017) 353-362.

[19] Z. Liu, G. Fu, J. Li, et al, Facile synthesis based on novel carbon-supported cyanogel of structurally ordered Pd_3Fe/C as electrocatalyst for formic acid oxidation, Nano Res. 11 (2018) 4686-4696.

[20] G. Fu, B. Xia, R. Ma, et al, Trimetallic PtAgCu@PtCu core@shell concave nanooctahedrons with enhanced activity for formic acid oxidation reaction, Nano Energy. 12 (2015) 824-832.

[21] X. Qiu, H. Zhang, P. Wu, et al, One-Pot Synthesis of Freestanding Porous Palladium Nanosheets as Highly Efficient Electrocatalysts for Formic Acid Oxidation, Adv. Funct. Mater. 27 (2017) 1603852.

[22] N. He, Y. Gong, Y. Yang, et al, An effective Pd@Ni-B/C anode catalyst for electro-oxidation of formic acid, Int. J. Hydrogen Energ. 43 (2018) 3216-3222.

[23] F. Li, Q. Xue, G. Ma, et al, Formic acid decomposition-inhibited intermetallic Pd_3Sn_2 nanonetworks for efficient formic acid electrooxidation, J. Power Sources. 450 (2020) 227615.

[24] J. Ren, J. Zhang, C. Yang, et al, Pd nanocrystals anchored on 3D hybrid architectures constructed from nitrogen-doped graphene and low-defect carbon nanotube as high-performance multifunctional electrocatalysts for formic acid and methanol oxidation, Materials Today Energy. 16 (2020) 100409.